INTERNATIONAL JOURNAL OF INTEGRATED ENGINEERING
ISSN: 2229-838X e-ISSN: 2600-7916

IJIE

Vol. 17 No. 8 (2025) 301-312
https://publisher.uthm.edu.my/ojs/index.php/ijie

Numerical Validation of Flexitank Hydrodynamic Performance under Different Driving Conditions

Mohamad Amirur Rahman Azahar[1], Nofrizalidris Darlis[2]*, Izuan Amin Ishak[2], Syafiqah Ruqaiyah Saiful Azam[1], Syabillah Sulaiman[2], Muhammad Adli Mustapa[3]

[1] *Faculty of Engineering Technology,*
Universiti Tun Hussein Onn Malaysia, Pagoh Education Hub, Panchor, Johor, 84600, MALAYSIA
[2] *Centre of Automotive & Powertrain Technology, Faculty of Engineering Technology,*
Universiti Tun Hussein Onn Malaysia, Pagoh Education Hub, Panchor, Johor, 84600, MALAYSIA
[3] *Maritime Engineering Technology Section,*
Universiti Kuala Lumpur Malaysian Institute of Marine Engineering Technology,
Lumut, Perak, 32200, MALAYSIA

*Corresponding Author: nofrizal@uthm.edu.my
DOI: https://doi.org/10.30880/ijie.2025.17.08.025

Article Info

Received: 12 September 2025
Accepted: 2 December 2025
Available online: 31 December 2025

Keywords

Flexitank, computational fluid dynamics (CFD), sloshing dynamics, hydrodynamic pressure, validation study, bulk liquid transport

Abstract

Flexitanks have revolutionized bulk liquid logistics through their cost-effectiveness and adaptability, yet their inherent flexibility introduces complex hydrodynamic challenges, particularly due to liquid sloshing during dynamic vehicle motion. This study presents a numerical validation of flexitank hydrodynamic performance under realistic driving conditions, focusing on the pressure response and fluid motion within the flexible containment. A 1:8 scaled flexitank prototype was experimentally tested to measure transient wall pressures and deformation using force-sensitive resistor (FSR) sensors, while a computational fluid dynamics (CFD) model was developed in Ansys Fluent to simulate the internal flow behavior. Comparison between experimental and numerical results demonstrated strong correlation, achieving a percentage different error below 8.5% throughout the driving cycle. The analysis further revealed that deceleration events generated 14-18% higher wall pressures than acceleration phases due to inertial and pressure wave effects. The validated CFD framework provides a reliable predictive tool for understanding sloshing-induced behavior in flexible liquid containment systems and contributes to safer, more efficient bulk liquid transport design.

1. Introduction

The global logistics sector is expanding, with bulk liquid transport crucial in international trade. Flexitanks, flexible containers placed inside shipping containers, offer a cost-effective, adaptable, and lightweight alternative to traditional ISO tanks, intermediate bulk containers, and drums. However, their flexible nature and the dynamic behaviour of contained liquids pose specific operational challenges. During acceleration, deceleration, or turning, common in heavy-duty truck operations, the liquid sloshes, creating substantial hydrodynamic forces [1]-[3]. These forces can increase internal pressure, cause localised stresses, and deform the tank walls, potentially leading to structural damage, leaks, or compromised vehicle stability [4], [5].

Sloshing and its associated hydrodynamic impacts are most critical during braking, often causing peak stress on the front flexitank walls [6]. Previous studies have explored liquid sloshing using both computational and

experimental approaches. Numerical methods such as Computational Fluid Dynamics (CFD) and Smoothed Particle Hydrodynamics (SPH) have been widely employed to predict free-surface behavior and pressure distribution. However, most studies focused on rigid-walled tanks or idealized boundary conditions, which fail to represent the complex deformation characteristics of flexible polymer materials used in flexitanks [7], [8]. Furthermore, recent works have emphasized the need for validation of numerical predictions against realistic dynamic conditions, yet few have achieved experimental correlation to verify simulation accuracy [3], [5].

Research into liquid motion in partially filled road containers has further highlighted the impact of sloshing on vehicle dynamics and stability [9], [10]. Early work by Romero et al. [11] Included experimental assessments of lateral sloshing forces in scaled road tankers, considering fill levels and container shapes, while Toumi et al. [12] Also provided analytical models for longitudinal sloshing. Another significant contribution comes from the extensive use of computational methods to simulate liquid behaviour. Qiong et al. [13], and Mi-An et al. [14], among others, have utilised Computational Fluid Dynamics to model liquid motion and hydrodynamic pressure distribution in various tank geometries. Additionally, Smoothed Particle Hydrodynamics, a mesh-free Lagrangian method, has been employed by researchers like Zhe Sun et al. [15], and Ersin [16], for analysing highly deformable systems like liquid sloshing, often coupled with finite element methods for fluid-structure interaction problems. Experimental validation of numerical models is essential for ensuring simulation accuracy. Without it, models may inaccurately represent sloshing forces, deformation, or stress concentrations.

Thus, this paper presents a validation study in which numerical simulations of flexitank hydrodynamics are compared against in-vehicle experimental data. A scaled-down flexitank prototype was mounted on a vehicle and instrumented to capture pressure responses and deformation patterns during realistic driving conditions. The corresponding CFD model was subjected to identical driving inputs. By comparing numerical predictions with experimental data, the accuracy of the numerical approach is assessed, thereby providing a validated framework for future full-scale flexitank studies and design improvements.

2. Materials and Methods

2.1 Geometry Modelling

The geometry of the flexitank used in this study was constructed based on the specifications reported by MY Flexitank Industries Sdn. Bhd. and follows the modelling approach presented by Mohamad et al. [3]. A three-dimensional geometry was developed in SolidWorks and later imported into ANSYS Fluent for numerical simulations. The reference full-scale flexitank has a rated capacity of 21,000 L with dimensions of 3028 mm (length) × 2362 mm (width) × 2223 mm (peak height). Fig. 1 shows the geometry model of the flexitank created using SolidWorks CAD software.

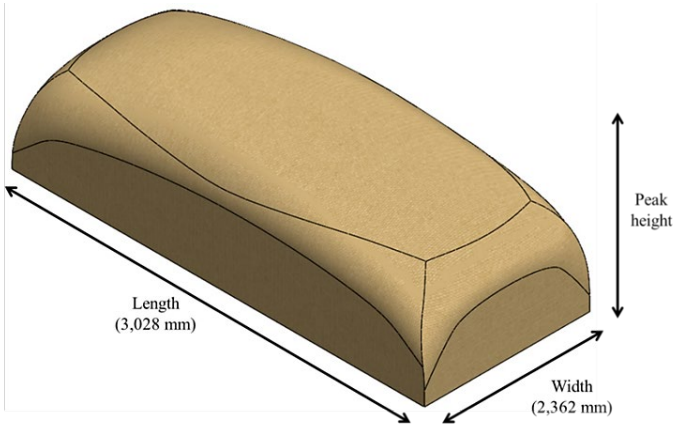

Fig. 1 *Flexitank model*

A scale factor of 1:8 was applied to the geometry to replicate the scaled-down in-vehicle experimental setup for validation. The scaled model preserved the geometric similarity of the full-scale flexitank while reducing the overall dimensions and capacity proportionally. This scaling ensured dynamic similarity in Froude number, allowing meaningful comparison between numerical and experimental results. Table 1 compares the full-scale flexitank and the 1:8 scaled-down model used for validation. Consequently, the scaled model capacity is reduced from 21,000 L to approximately 41 L, making it feasible for in-vehicle experimental testing while maintaining the hydrodynamic characteristics necessary for meaningful comparison with the full-scale numerical model.

Int. Journal of Integrated Engineering Vol. 17 No. 8 (2025) p. 301-312

In this study, water was selected as the reference fluid due to its well-documented physical properties and availability for validation testing. The density (ρ) and dynamic viscosity (μ) were assigned as 997 kg/m^3 and 0.001 kg/m·s, respectively, based on standard fluid property values at room temperature (25 °C) [3]. These properties were incorporated into the CFD solver to represent fluid behaviour accurately during transient sloshing conditions.

Table 1 *Comparison of full-scale and scaled-down geometry*

Parameter	Full-scale model	Scaled-down model (1:8)
Capacity (L)	21,000	41
Length (mm)	3028	379
Width (mm)	2362	295
Peak height (mm)	2223	278

The flexitank wall material was modelled using linear low-density polyethene (LLDPE), which is commonly employed in commercial flexitank manufacturing due to its high flexibility, chemical resistance, and durability. The flexitank was simplified for numerical simulations as a single 0.3048 mm-thick LLDPE layer, representing the actual multilayer construction used in practice. The mechanical properties of LLDPE, such as density, Young's modulus, Poisson's ratio, and yield strength, were obtained from a combination of tensile testing and literature values [17]. The tensile tests were explicitly performed to generate accurate stress–strain data, which were then used as direct input for defining the material properties in the simulation model. By integrating experimentally measured material parameters into the solver, the numerical predictions of flexitank deformation and stress distribution under hydrodynamic loading were made more realistic and representative of the prototype material.

2.2 Numerical Procedure

This study simulated the model using CFD software, Ansys Fluent, to analyse hydrodynamic performance for various filling volume capacities and fluid densities. A SIMPLE discretisation of pressure-velocity coupling is chosen, which makes equation convergence difficult but increases solution precision. The k–ω SST turbulence model and scalable wall function are used.

The k–ω SST turbulence model can solve turbulence parameters near the wall region, where an adverse pressure gradient is developed [18]. Using Ansys software, the model was developed by coupling a fluid flow solver with a mechanical solver. An interface established the connection between the fluid and structural domains within these two solvers. Fig. 2 illustrates the computational domain used in this study. In the fluid domain, the model's outer face is considered a fluid wall. The fixed support of the model was represented by the surface that fully meets the container body. Meanwhile, the solid domain's outer wall is considered the fluid-solid interface where the imported pressure from the fluid domain is attached.

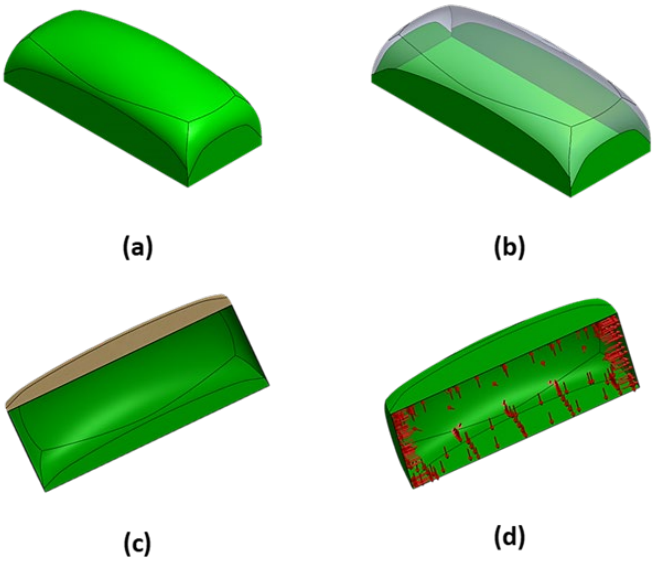

Fig. 2 *The boundary conditions for (a) Fluid wall; (b) Fixed support; (c) Fluid-solid interface; (d) Imported pressure from fluid solver*

Due to the model's simplicity, it was meshed using the hexahedron approach. The purpose is to reduce numerical diffusion and aiding convergence. The Ansys Advanced Meshing module was used to generate a structured hexa-dominant mesh. To analyse mesh independence, three different mesh resolutions are considered, including coarse, medium, and fine mesh types. After performing the grid independence test, the medium mesh type with 40 mm of element size and 1.2 growth rate, resulting 830,000 number of elements was selected for all subsequent simulations. This mesh provided a balance between accuracy and computational efficiency, as the variation in average wall pressure between the medium and fine meshes was less than 1%, indicating mesh convergence. Furthermore, the medium mesh reduced computational cost by nearly 50% compared to the fine mesh, without compromising result reliability. Therefore, the medium mesh configuration was adopted as the reference model for all CFD analyses in this study.

The numerical simulation and the scaled-down in-vehicle experiment were subjected to representative driving profiles to ensure consistency in validation. Two types of profiles were considered in this study. The first profile was derived from the West Virginia University (WVU) Heavy-Duty Truck Cycle, focusing on a braking event where the vehicle decelerates from approximately 16 km/h to a complete stop within six seconds [19]. This profile was implemented as a transient boundary condition in the CFD solver to evaluate hydrodynamic performance under standardised heavy-duty conditions.

The second profile was obtained from an actual in-vehicle test using a GPS data logger to collect real-time velocity data during the scaled-down flexitank experiment. The velocity and time history from the logger captured both acceleration and braking phases, as shown in Fig. 3. This experimental profile was also applied to the numerical model to ensure that the simulation conditions closely replicated those encountered during physical testing. By employing a standardised driving cycle and an experimentally measured driving profile, the study ensured that the numerical model was validated under controlled conditions while also reflecting realistic vehicle dynamics. This dual approach allowed for a comprehensive assessment of the model's predictive capability.

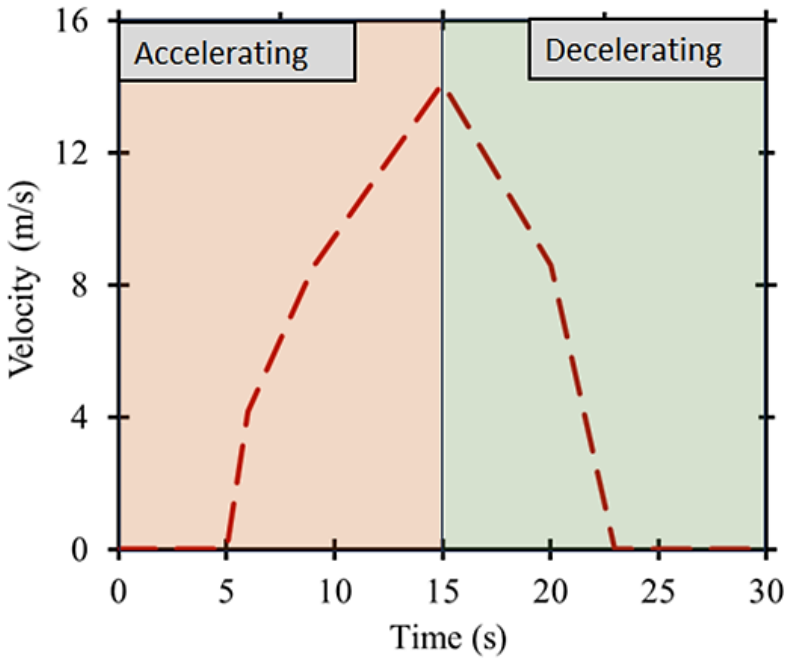

Fig. 3 *Velocity profile obtained from the GPS data logger*

2.3 Experimental Setup

An in-vehicle experiment was conducted to measure hydrodynamic behaviour induced by sloshing fluid inside a scaled-down flexitank for numerical validation. The experiment was performed on campus road at Universiti Tun Hussein Onn Malaysia, Pagoh Campus, Johor, Malaysia. This experiment collected data from the Force Sensitive Resistor (FSR) sensor attached to a scaled-down flexitank. The data will then be compared with the CFD simulation to validate the numerical setup.

An FSR sensor is connected to the Arduino UNO as shown in Fig. 4. The positive lead of FSR is connected to the 5V pin on the Arduino, while the negative lead is connected to a digital pin. A 56K resistor is used as a pull-down resistor to ensure the digital pin reads a low value when the FSR is not pressed. Then, a code created in Arduino IDE is uploaded to Arduino UNO to monitor the value. This value is not the actual reading needed; it's a

Int. Journal of Integrated Engineering Vol. 17 No. 8 (2025) p. 301-312

raw value from the analogue-to-digital converter of the Arduino. A calibration needs to be done on the sensor to convert the reading to an actual one.

Calibrating an FSR sensor involves using a known weight to apply a specific amount of force to the sensor and then recording the sensor's output value. This process is repeated multiple times with different weights, and the results are plotted on a graph. These output values are then used to calculate a calibration factor that can be applied to future readings to convert them into an accurate force measurement, achieving a linear correlation coefficient of $R^2 = 0.995$ with an uncertainty of ±2.1%. The slope of the line from this graph is the calibration factor used to convert future readings into precise force measurements. The process is repeated for different pressure points on the sensor to ensure it is calibrated correctly.

The experimental setup for this study consisted of a scaled-down flexitank, which was used to mimic the behaviour of a full-scale flexitank. The flexitank was filled with water, and the pressure distribution within the tank was measured using FSR sensors. The FSR sensors were attached to the flexitank at the top-back of the flexitank, as shown in Fig. 5, to capture the pressure distribution throughout the package. The experiment would involve driving the Perodua Viva on a predetermined test route that simulates different driving conditions, such as braking, accelerating, and turning. The sensor data would be recorded during the experiment, allowing for the measurement of the behaviour of the fluid within the flexitank under these different conditions. A GPS data logger is used to collect vehicle data, such as velocity, during an in-vehicle experiment of a flexitank. The data collected from the sensors was then analysed and compared to the results from a CFD simulation of the same system.

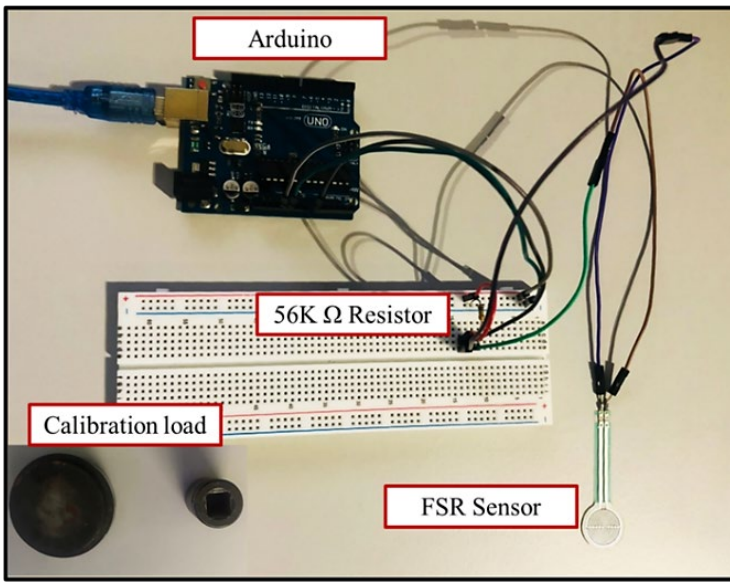

Fig. 4 *Pressure sensor setup*

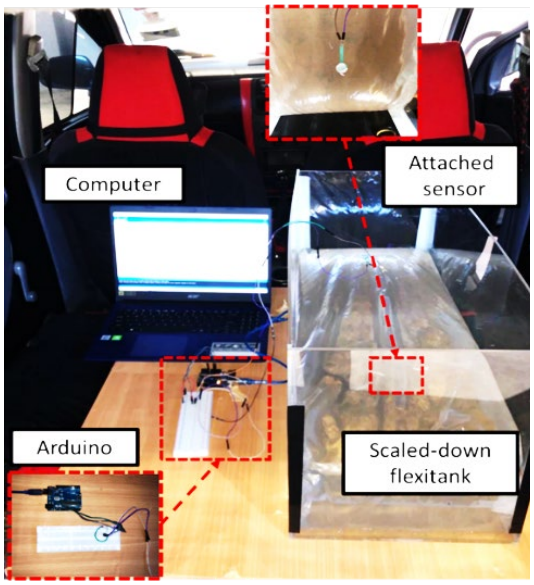

Fig. 5 *Experimental setup*

3. Results and Discussion

3.1 Grid Independence Test

Grid independence is the term used to describe the improvement of results by using successively smaller cell sizes for the calculations. A calculation should approach similar results as the mesh becomes finer, hence the term grid independence. Fig. 6 shows the wall shear for 21,000 L flexitank size model with three different mesh resolutions. Hence, the sizing of the mesh was increased approximately from the node of 75 K to 450 K nodes to observe the significant changes of the velocity. Based on the grid independence test, there are no significant changes of the wall shear numbers with average relative error below 1% in velocity from the medium (150 K nodes) to fine (450 K nodes). Thus, the subsequent simulations are set approximately equal or greater to 150 K nodes. As this model achieves grid independence, the cell size should be successively smaller to minimize error due to discretization and utilizing the same mesh setting on the other models.

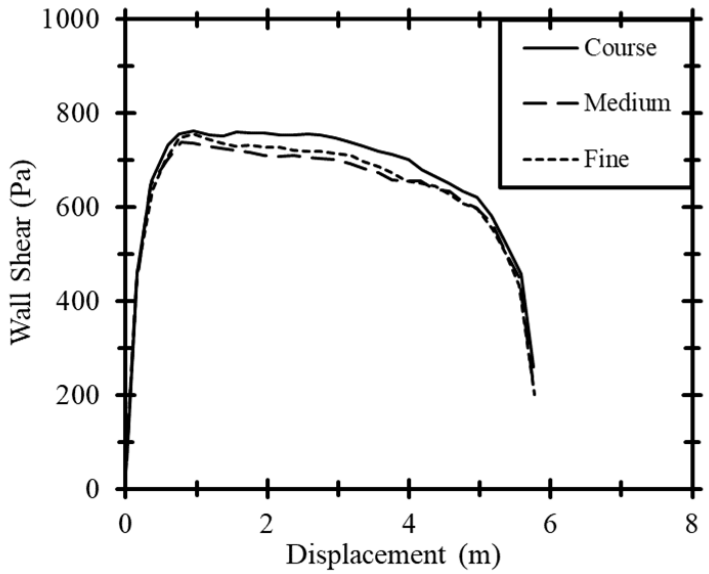

Fig. 6 *Grid independence test result for three different mesh parameters*

3.2 Mechanical Behavior of Linear Low-Density Polyethylene

The tensile test on the 12 Mil (0.3048 mm) LLDPE specimen was carried out to characterise the material properties used in the flexitank. The representative stress–strain curve is shown in Fig. 7, where the material exhibits an initial elastic region, followed by yielding and subsequent strain hardening before final fracture. The failure is indicated by a sudden drop in stress after reaching the ultimate tensile strength.

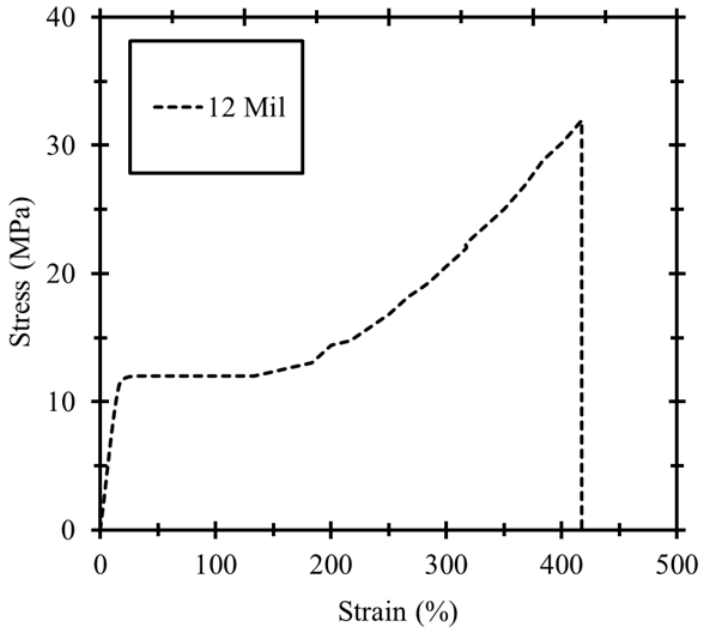

Fig. 7 *Typical stress-strain curves of the LLDPE samples*

The mechanical properties obtained from the tensile test are summarised in Table 2. For the 12 Mil LLDPE, the Young's modulus was measured at 68.88 MPa, the yield stress at 14.76 MPa, the strain at yield at 16.45%, and the strain at break at 421%. These values confirm that the material has significant ductility and strength, making it suitable for flexitank applications. The relatively high yield stress and significant elongation at break suggest that 12 Mil LLDPE can withstand the internal stresses induced by liquid sloshing and external pressures during transport without experiencing permanent deformation. This combination of strength and flexibility ensures reliable performance under dynamic loading conditions.

Int. Journal of Integrated Engineering Vol. 17 No. 8 (2025) p. 301-312

Table 2 *Mechanical properties of the LLDPE samples*

Sample	Young's modulus (MPa)	Yield stress (MPa)	Strain at yield (%)	Strain at break (%)
12 Mil (0.3048 mm)	68.88	14.76	16.45	421.00

3.3 Numerical Validation with Experimental Data

The CFD result was validated by comparing the pressure on the outer surface at the top (back) of the scaled-down flexitank package. Fig. 8 compares numerical and experimental pressure under a transient driving profile. The dashed red line indicates the velocity profile used as the excitation input, while the solid black line and markers denote the CFD predictions and experimental measurements, respectively.

The pressure trends clearly follow the variations in vehicle dynamics. During acceleration phases, both CFD and experimental results show a sharp rise in pressure. This can be attributed to the inertial response of the liquid mass, which shifts toward the rear wall of the flexitank, thereby generating a sudden increase in hydrostatic and dynamic loading on the monitored surface. As the velocity reaches a near-steady condition, the inertial forcing diminishes, allowing the liquid to redistribute and the pressure to stabilize at an intermediate level. Conversely, during deceleration, the fluid continues its forward motion due to inertia while the tank experiences a retarding force. This causes the rear surface to be relieved of significant fluid loading, leading to a rapid pressure reduction that approaches zero as the vehicle comes to rest. Negligible inertial effects are present at stationary intervals, and only residual sloshing is observed, resulting in near-zero measured pressures.

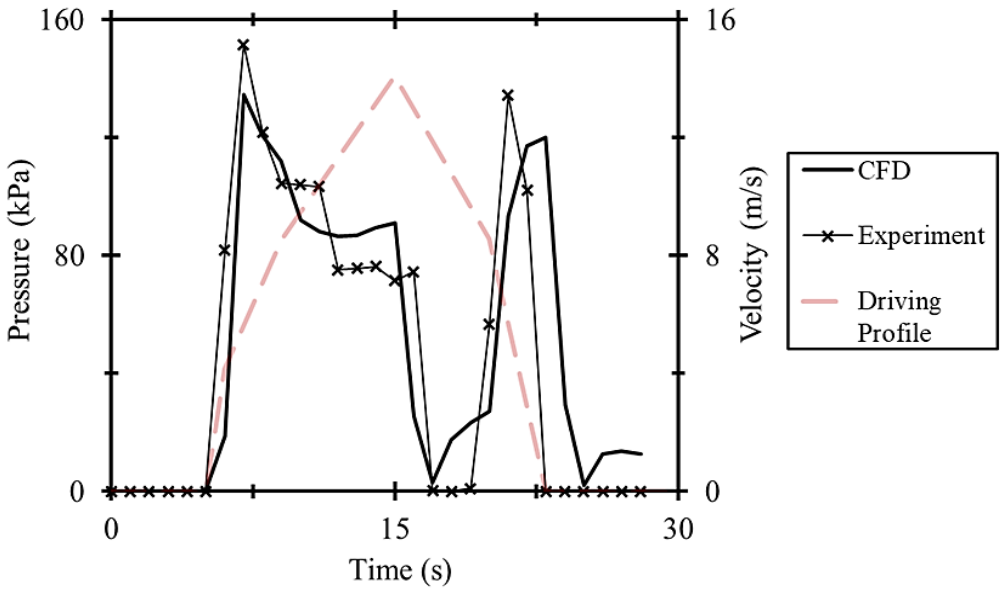

Fig. 8 *Pressure values for both numerical and experimental*

The CFD model successfully reproduces these dynamic characteristics, with simulation results closely following the experimental measurements across all driving phases. Minor discrepancies are observed at peak pressures and transition periods, which may be attributed to experimental uncertainties and modelling assumptions such as turbulence representation and mesh resolution. Nevertheless, quantitative assessment through relative error analysis confirms that the deviation remains below 8.5% throughout the entire driving cycle, as shown in Table 3. This level of agreement validates the robustness of the CFD framework and supports its applicability for predictive analyses of flexitank performance under dynamic loading conditions.

Table 3 *Mechanical properties of the LLDPE samples*

	Experiment	CFD
Average	44.83	48.85
Relative error (%)	8.23	

3.4 Effects of Critical Driving Condition on Flexitank

Hydrodynamics is concerned with the study and description of fluids in motion. The primary focus is on imparting an understanding of the principles governing the conservation of mass, energy, and momentum. Flowing fluids possess kinetic energy. This energy can be converted into potential energy (pressure, height) and vice versa. Hydrodynamics can be used to model and predict the behaviour of liquids in a flexitank, including the amount and frequency of sloshing that may occur. Sloshing is a phenomenon that occurs when liquids move inside a flexitank due to changes in the container's motion or acceleration. The movement of liquids in a flexitank is affected by the physical properties of the liquid, such as its density and viscosity, as well as the shape and size of the flexitank.

The critical driving condition is the speed at which the amplitude of the sloshing waves inside a container reaches its maximum. This is the speed at which the container is most prone to sloshing and the speed at which the largest amount of sloshing will occur. When a flexitank is being transported in a vehicle, the speed of the vehicle, as well as the type of road surface and the quality of the suspension system, can all affect the critical driving condition. If the vehicle travels at or near the critical speed, the sloshing inside the flexitank can become more severe, increasing the risk of damage to the flex tank.

Numerous studies claimed that deceleration produces much higher pressures compared to the acceleration scenario [20]-[25]. Hence, it is important to consider the critical driving conditions when transporting flexitank, and to avoid traveling at or near the critical speed. Fig. 9 compares average pressure acted on flexitank for three fluids with different densities under similar driving profiles. When the motion is accelerating, the effect on the liquid in the flexitank is less severe because the acceleration is gradual, and the liquid has time to adjust to the change in motion. However, when a vehicle suddenly brakes, the direction of motion changes abruptly, which can cause the liquid in the flexitank to move in the opposite direction, increasing sloshing. Thus, it is essential to note that braking should be done gradually and with enough distance from the stop point to prevent excessive sloshing.

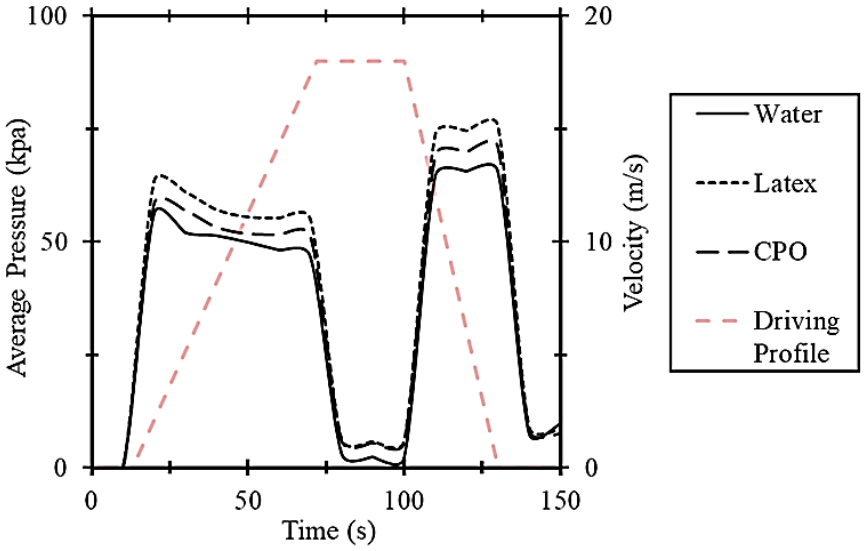

Fig. 9 *Average pressure comparison between different fluid density*

Table 4 indicates the pressure contour of different fluid densities based on a specific time, where the moving direction of the flexitank is based on the positive x-axis direction. For the first 70 seconds, the flexitank is in an initial accelerating condition. At this period, all contours show that the pressure is in the opposite direction of vehicle motion. While looking at the blue colour pressure range, it showed that negative sign of the pressure value. In hydrodynamics, when a vehicle is accelerating, the pressure acting on the vehicle is in the opposite direction of the motion due to the phenomenon of added mass effect [26]. When a vehicle accelerates, it creates a disturbance in the fluid around it, which in turn creates an additional force acting on the vehicle that is opposite to the direction of motion. This additional force, called the added mass effect, is a result of fluid inertia, and it acts as an opposing force to the acceleration of the vehicle.

Int. Journal of Integrated Engineering Vol. 17 No. 8 (2025) p. 301-312

Table 4 *Pressure distribution on flexitank structure for one driving cycle*

Fluid	Water	Latex	CPO
0 s	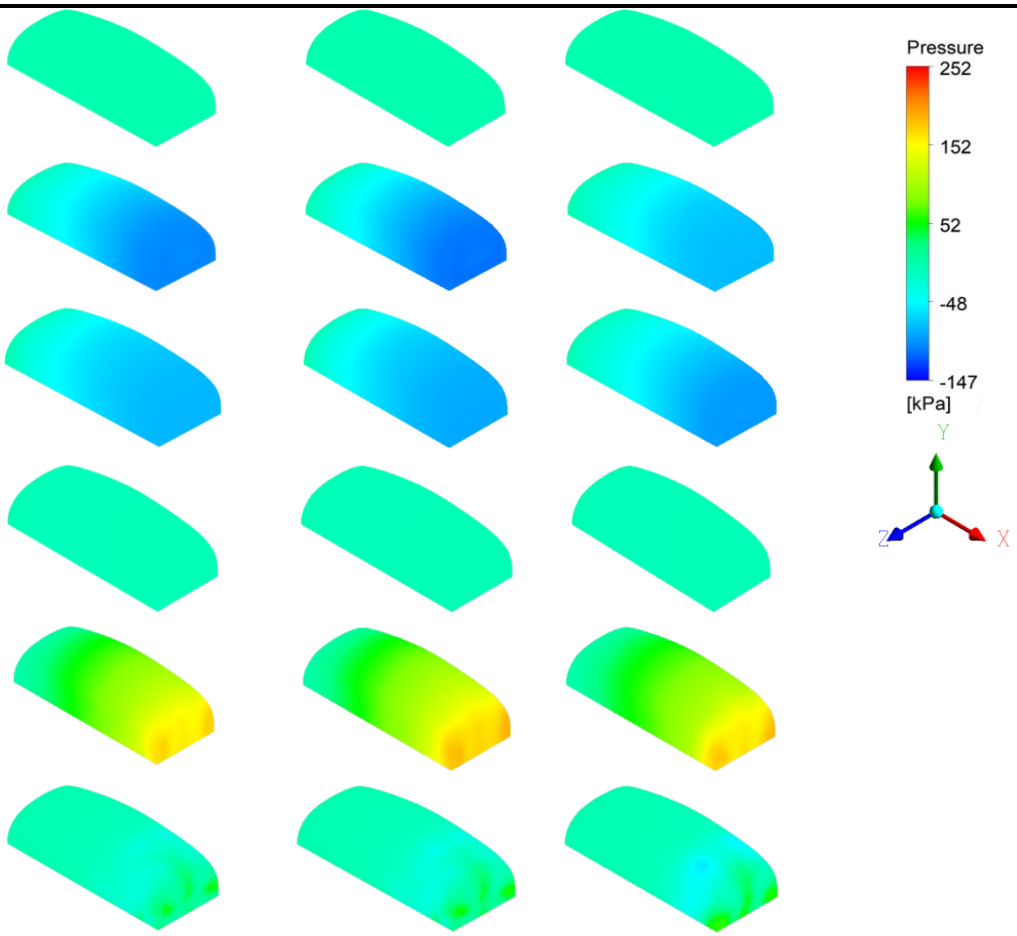		
30 s			
60 s			
90 s			
120s			
150 s			

After a vehicle reaches a constant velocity after accelerating in a fluid, the hydrodynamic pressure acting on the car will decrease and eventually get a steady state, as shown during 80 seconds to 100 seconds. The added mass effect caused by the acceleration of the fluid around the vehicle will dissipate as the vehicle reaches a constant velocity, and the pressure acting on the vehicle will return to the normal drag force caused by the fluid resistance. In other words, as the vehicle's velocity becomes constant, the added mass effect will stop, and the hydrodynamic pressure will be only due to the drag force, a function of the fluid density, viscosity, and the square of the velocity. Therefore, the hydrodynamic pressure will decrease to a steady state value when the vehicle reaches a constant velocity.

When braking is applied to a vehicle that is carrying fluid, the hydrodynamic pressure acting on the vehicle will change as the vehicle's velocity decreases. The drag force, which was acting in the opposite direction of the motion, will still be present, but it will decrease as the velocity of the vehicle decreases. In addition to the drag force, the vehicle braking will also create a phenomenon known as the "pressure wave" that can cause an increase in the hydrodynamic pressure on the vehicle [27], [28]. This pressure wave is caused by the abrupt change in velocity of the vehicle, and it can cause an increase in the pressure on the front of the vehicle as it slows down, producing 14%-18% more pressure compared to the accelerating condition.

As a vehicle suddenly brakes, the front of the vehicle slows down more quickly than the fluid around it. This creates a region of high-pressure fluid in front of the vehicle, and a region of low-pressure fluid behind it. This high-pressure region then propagates through the fluid as a wave, creating a pressure wave on the front of the vehicle. The magnitude of the pressure wave depends on the rate of deceleration, the density and viscosity of the fluid. The sloshing forces can cause stress on the flexitank structure, which can lead to deformation or even failure of the flexitank if the forces are large enough [29], [30].

4. Conclusions

This study presented a numerical validation of flexitank hydrodynamic performance under realistic vehicle driving conditions. A 1:8 scaled-down prototype was experimentally tested to measure transient pressure

responses using calibrated FSR sensors, and the results were compared with CFD simulations developed in ANSYS Fluent.

The findings demonstrated strong agreement between simulation and experimental data, with a percentage different below 8.5%, confirming the predictive accuracy of the CFD model. The results also revealed that deceleration conditions generated 14-18% higher wall pressures compared to acceleration due to fluid inertia and pressure wave reflection.

The validated CFD framework provides a reliable tool for predicting hydrodynamic pressures and can be applied to design optimization of flexitank wall thickness, baffle placement, and overall structural safety. This work contributes to a better understanding of liquid sloshing behavior under transient motion, supporting safer and more efficient bulk liquid transport operations. Future research will extend this validation approach to full-scale flexitanks and include the effect of baffle geometry to further mitigate pressure peaks and wall deformation.

Acknowledgement

This research was supported by Universiti Tun Hussein Onn Malaysia (UTHM) through Tier 1 Grant (vot Q968). The author would like to thank the Faculty of Engineering Technology, UTHM, for providing the necessary research facilities for this study.

Conflict of Interest

Authors declare that there is no conflict of interests regarding the publication of the paper.

Author Contribution

The authors confirm contribution to the paper as follows: ***study conception and design:*** *Mohamad Amirur Rahman Azahar, Nofrizalidris Darlis, Muhammad Adli Mustapa;* ***data collection:*** *Mohamad Amirur Rahman Azahar,* Syafiqah Ruqaiyah Saiful Azam, *Syabillah Sulaiman;* ***analysis and interpretation of results:*** *Mohamad Amirur Rahman Azahar, Izuan Amin Ishak;* ***draft manuscript preparation:*** *Mohamad Amirur Rahman Azahar, Nofrizalidris Darlis, Syafiqah Ruqaiyah Saiful Azam. All authors reviewed the results and approved the final version of the manuscript.*

References

[1] K. Ren, G. X. Wu & Z. F. Li (2021) Natural modes of liquid sloshing in a cylindrical container with an elastic cover, *Journal of Sound and Vibration*, *512*, 116390, https://doi.org/10.1016/j.jsv.2021.116390

[2] Konstantinos N., Androutsopoulos & Konstantinos G. Zografos (2024) Modeling and solving the fuel distribution problem with unloading precedence and loading sequence considerations, *Annals of Operations Research, 332(1)*, 909-947, https://doi.org/10.1007/s10479-023-05752-1

[3] Mohamad Amirur Rahman Azahar, Nofrizalidris Darlis, Norhafizzah Hassan, Zuliazura Mohd Salleh, Syafiqah Ruqaiyah Saiful Azam, Ishkrizat Taib, Mohd Zamani Ngali, Khairul Nizam Mustaffa & Muhamad Mohshein Hashim, CFD analysis on different filling volume capacity and fluid density for flexitank application, *CFD Letters, 15(1)*, 1-12, https://doi.org/10.37934/cfdl.15.1.115126

[4] M. Toumi, Bouazara, M., & Richard, M. J. (2009) Impact of liquid sloshing on the behaviour of vehicles carrying liquid cargo, *European Journal of Mechanics-A/Solids*, 28(5), 1026-1034, https://doi.org/10.1016/j.euromechsol.2009.04.004

[5] Muhammad Haidir Hamdan, Nofrizalidris Darlis, Yong Tze Mi, Izuan Amin Ishak, Syabillah Sulaiman, Md Norrizam Mohmad Ja'at, Abd Fathul Hakim Zulkifli, Khairul Nizam Mustafa & Muhamad Mohshein Hashim (2022) Hydrodynamics analysis on liquid bulk transportation with different driving cycle conditions, *Journal of Advanced Research in Fluid Mechanics and Thermal Sciences, 100(1)*, 137-151, https://doi.org/10.37934/arfmts.100.1.137151

[6] Mengmeng Han, Jian Dai, Chien Ming Wang & Kok Keng Ang (2019) Hydrodynamic analysis of partially filled liquid tanks subject to 3d vehicular manoeuvring, *Shock and Vibration, 2019(1)*, 6943879, https://doi.org/10.1155/2019/6943879

[7] S. Nicolici &R. M. Bilegan (2013) Fluid structure interaction modeling of liquid sloshing phenomena in flexible tanks, *Nuclear Engineering and Design, 258*, 51-56, https://doi.org/10.1016/j.nucengdes.2012.12.024

[8] R. S. Ganuga, Harish Viswanathan, S. Sonar & A. Awasthi (2014) Fluid-structure interaction modelling of internal structures in a sloshing tank subjected to resonance, *International Journal of Fluid Mechanics Research, 41(2)*, 145-168, https://doi.org/10.1615/InterJFluidMechRes.v41.i2.40

[9] Ling Hou, Fangcheng Li & Chunliang Wu (2012) A numerical study of liquid sloshing in a two-dimensional tank under external excitations, *Journal of Marine Science and Application, 11(3)*, 305-310, https://doi.org/10.1007/s11804-012-1137-y

[10] Hyunjong Kim, Nanjundan Parthasarathy, Yoon-Hwan Choi & Yeon-Won Lee (2018) Reduction of sloshing effects in a rectangular tank through an air-trapping mechanism–a numerical study, *Journal of Mechanical Science and Technology,* 32(3), 1049-1056, https://doi.org/10.1007/s12206-018-0206-9

[11] J. A. Romero, O. Ramírez, J. M. Fortanell, M. Martinez & A. Lozano (2006) Analysis of lateral sloshing forces within road containers with high fill levels, *Proceedings of the Institution of Mechanical Engineers, Part D: Journal of Automobile Engineering, 220(3)*, 303-312, https://doi.org/10.1243/09544070JAUTO42

[12] M. Toumi, M. Bouazara & M. J. Richard (2008) Analytical and numerical analysis of the liquid longitudinal sloshing impact on a partially filled tank-vehicle with and without baffles, *International Journal of Vehicle Systems Modelling and Testing, 3(3)*, 229-249, https://doi.org/10.1504/IJVSMT.2008.023840

[13] Qiong Zhang, Hanhua Zhu & Wei Wei (2021) Numerical simulation on the sloshing characteristics of gasliquid flow in cargo tank and anti-sloshing methods, In *Journal of Physics: Conference Series*, *1746(1)*, 012046, IOP Publishing, https://doi.org/10.1088/1742-6596/1746/1/012046

[14] Mi-An Xue, Yichao Chen, Jinhai Zheng, Ling Qian & Xiaoli Yuan (2019) Fluid dynamics analysis of sloshing pressure distribution in storage vessels of different shapes, *Ocean Engineering, 192*, 106582, https://doi.org/10.1016/j.oceaneng.2019.106582

[15] Zhe Sun, Yi-chen Jiang, Gui-yong Zhang, Zhi Zong, Jing Tang Xing & Kamal Djidjeli (2019) Slamming load on trimaran cross section with rigid and flexible arches, *Marine Structures, 66*, 227-241, https://doi.org/10.1016/j.marstruc.2019.04.010

[16] A. Ersin Dincer, (2019) Investigation of the sloshing behavior due to seismic excitations considering two-way coupling of the fluid and the structure, *Water,* 11(12), 2664, https://doi.org/10.3390/w11122664

[17] Luděk Hynčík, Petra Kochová, Jan Špička, Tomasz Bońkowski, Robert Cimrman, Sandra Kaňáková, Radek Kottner & Miloslav Pašek (2021) Identification of the lldpe constitutive material model for energy absorption in impact applications, *Polymers, 13(10)*, 1537, https://doi.org/10.3390/polym13101537

[18] Rocha, PA Costa, HH Barbosa Rocha, FO Moura Carneiro, ME Vieira Da Silva & A. Valente Bueno. "k–ω SST (shear stress transport) turbulence model calibration: A case study on a small-scale horizontal axis wind turbine, *Energy, 65*, 412-418, https://doi.org/10.1016/j.energy.2013.11.050

[19] Nigel N. Clark, J. Todd Messer, David L. McKain, Wenguang Wang, Reda M. Bata, Mridul Gautam, & Donald W. Lyons (1995) Use of the West Virginia University truck test cycle to evaluate emissions from class 8 trucks, *SAE Transactions*, *104*, 1-13, https://doi.org/10.4271/951016

[20] Yunus A. Cengel, & John M. Cimbala (2006) *Fluid kinematics*, Fluid Mechanics Fundamentals and Applications (pp. 121-170) Mc Graw Hill Higher Education.

[21] Joel H. Ferziger & Milovan Perić (2002) *Solution of the Navier-Stokes equations*. In *Computational methods for fluid dynamics* (pp. 157-216) Berlin, Heidelberg: Springer Berlin Heidelberg.

https://doi.org/10.1007/978-3-642-56026-2_7

[22] Hafsa Mir, Tahir Abdul Hussain Ratlamwala, Ghulam Hussain, Mohammed Alkahtani & Mustufa Haider Abidi (2020) Impact of sloshing on fossil fuel loss during transport, *Energies, 13(10)*, 2625, https://doi.org/10.3390/en13102625

[23] Rajamani Rajagounder, Guru Vignesh Mohanasundaram & Prakasan Kalakkath (2016) A study of liquid sloshing in an automotive fuel tank under uniform acceleration, *Engineering Journal,* 20(1), 71-85, https://doi.org/10.4186/ej.2016.20.1.71

[24] Borg, Mitchell G., Claire DeMarco Muscat-Fenech, Tahsin Tezdogan, Tonio Sant, Simon Mizzi & Yigit Kemal Demirel, A numerical analysis of dynamic slosh dampening utilising perforated partitions in partially-filled rectangular tanks, *Journal of Marine Science and Engineering*, *10(2)*, 254,

https://doi.org/10.3390/jmse10020254

[25] S. W. Zhou & Z. H. Liu. (2019) Simulation analysis of liquid sloshing under different working conditions of hazardous materials rescue truck, In *IOP Conference Series: Materials Science and Engineering*, *657(1)*, 012017, IOP Publishing, https://doi.org/10.1088/1757-899X/657/1/012017

[26] You-Hong Eng, Cheng-Siong Chin & Michael Wai-Shing Lau (2014) Added mass computation for control of an open-frame remotely-operated vehicle: Application using WAMIT and MATLAB, *Journal of Marine Science and Technology, 22(4)*, 1.

[27] Gao, Dinggang, Fei Ni, Guobin Lin, Shihui Luo & Wen Ji (2019) Aerodynamic analysis of pressure wave of high-speed maglev vehicle crossing: Modeling and calculation, *Energies, 12(19)*, 3770, https://doi.org/10.3390/en12193770

[28] Guihui Ma, Fu Chen, Jianyang Yu, Yanping Song & Zenan Mu (2018) Effect of pressure-equalizing film on hydrodynamic characteristics and trajectory stability of an underwater vehicle with injection through one or two rows of venting holes, *Journal of Fluids Engineering, 140(9)*, 091103,

https://doi.org/10.1115/1.4039519

[29] Soorya Elizabath G. & Sheeja Janardhanan (2007) Estimation of structural strength of tanks under sloshing loads, *International Journal of Innovative Research in Science, Engineering and Technology*, *5(9)*, 16037-16050,

[30] Chih-Hua Wu, Bang-Fuh Chen & Tin-Kan Hung (2013) Hydrodynamic forces induced by transient sloshing in a 3D rectangular tank due to oblique horizontal excitation, *Computers & Mathematics with Applications, 65(8)*, 1163-1186, https://doi.org/10.1016/j.camwa.2013.02.012